



HAL
open science

Evidence of Large Infrasonic Radiation Induced by Earthquake Interaction with Alluvial Sediments

E. Marchetti, G. Lacanna, A. Le Pichon, D. Piccinini, M. Ripepe

► **To cite this version:**

E. Marchetti, G. Lacanna, A. Le Pichon, D. Piccinini, M. Ripepe. Evidence of Large Infrasonic Radiation Induced by Earthquake Interaction with Alluvial Sediments. *Seismological Research Letters*, 2016, 87 (3), pp.678-684. 10.1785/0220150223 . cea-02107025

HAL Id: cea-02107025

<https://cea.hal.science/cea-02107025>

Submitted on 23 Apr 2019

HAL is a multi-disciplinary open access archive for the deposit and dissemination of scientific research documents, whether they are published or not. The documents may come from teaching and research institutions in France or abroad, or from public or private research centers.

L'archive ouverte pluridisciplinaire **HAL**, est destinée au dépôt et à la diffusion de documents scientifiques de niveau recherche, publiés ou non, émanant des établissements d'enseignement et de recherche français ou étrangers, des laboratoires publics ou privés.

1
2
3
4
5
6
7
8
9
10
11
12
13
14
15
16
17
18
19
20
21
22
23

Evidence of large infrasonic radiation induced by earthquake interaction with alluvial sediments.

E. Marchetti¹, G. Lacanna¹, A. Le Pichon², D. Piccinini³, M. Ripepe¹.

- 1) Department of Earth Sciences, University of Firenze, via G. La Pira, 4, 50121, Firenze, Italy
- 2) CEA/DAM/DIF, F-91297 Arpajon, France
- 3) Istituto Nazionale di Geofisica e Vulcanologia, via della Faggiola, 32, 56126, Pisa, Italy

Abstract

The M_w 5.9 Ferrara earthquake that struck Northern Italy in May, 20th, 2012, was recorded with an infrasound array at a source-to-receiver distance of 300 km. The infrasound record revealed early and late detections characterized by large back-azimuth variations suggesting the existence of an extended area of infrasound radiation. Unlike most of previous studies, the modeled area of maximum infrasound radiation appears to mimic an extended flat area (plain of Po river) with no significant contributions from nearby mountain ranges. The shake map of the earthquake and the map of reported acoustic boom is in good agreement with the modeled area of infrasound radiation suggesting how the transition of seismic waves into acoustic atmospheric waves is efficiently exciting infrasound recorded at far distances from the source. Such a result is in agreement with the significant seismic amplification within the Po plan alluvial sediments.

24

25

26

27

28 **1. Introduction**

29 Earthquakes are a well-known sources of atmospheric pressure waves [e.g. Mutschlecner and
30 Whitaker, 2005 for a review] that are inferred to be produced by three distinct possible source
31 mechanisms: (i) pressure changes due to the vertical displacement of the seismic waves near the
32 infrasound station, (ii) the local conversion from seismic waves to the sound pressure near the epicenter
33 area [Olson et al., 2003; Arrowsmith et al., 2009], and (iii) pressure waves generated in remote areas by
34 the seismic shaking of the topographic relief [e.g. Le Pichon et al., 2003; Mutschlecner and Withaker,
35 2005; Le Pichon et al., 2005; Green et al., 2009].

36 The latter kind of source mechanism, that is usually referred to as *secondary infrasound*, is
37 reported for a wide range of magnitudes, spanning from low magnitude ($M_L \sim 4$) shallow events [Green
38 et al., 2009] to mega earthquakes ($M_L > 8$), and is usually inferred to be strongly related to steep
39 topographical features [e.g. Le Pichon et al. 2002, 2005]. In particular, Green et al., [2009] modeled the
40 ground-to-air coupling of the 2007 Folkestone earthquake (UK) as being produced by the shaking of
41 the vertical coastal cliffs induced by the nearby (< 5 km epicentral distance) seismic event. Similarly,
42 Arrowsmith et al., [2009] identified from multiple array observations of an earthquake sequence in
43 Nevada a repeating secondary source as being produced by an isolated mountain peak (about 300 m
44 high).

45 In this study we present infrasound observations of the 2012, ML 5.9, Ferrara earthquake (Italy)
46 as recorded by a small aperture array deployed in the Northwestern Italian Alps at an epicentral
47 distance of ~ 300 km. Infrasound observations are used to infer the location and extent of the

48 infrasound radiant area, in terms of ground-to-atmosphere coupling of seismic waves, by considering
49 the seismic and infrasonic propagation from the source to the array. Our results suggest the existence of
50 an extended radiant area that appears to match the Po alluvial plan thus providing a new hypothesis on
51 the generation of infrasound from earthquakes.

52

53

54 **2. The seismic sequence**

55 On May 20, 2012, at 02:03 UTC, a 5.9 M_w earthquake occurred in the Po plain, Northern Italy,
56 west of the city of Ferrara at a hypocentral depth of 6.3 km (Figure 1: (a) Epicenter of the May, 20th,
57 2012 Ferrara earthquake (red star) and position of the CHA infrasound array (blue triangle) at a
58 distance of ~ 300 km from the earthquake epicenter. Raw infrasound data (b) and spectrogram
59 (c) recorded at the CHA array. (d) back-azimuth (ba) and apparent velocity (av) of infrasound
60 detections obtained for the infrasonic signal at the CHA array. Earthquake origin time (red line)
61 and celerity values that would correspond to early and late arrivals (410 and 205 m/s, blue lines)
62 are shown for reference.). The event caused 25 casualties and extensive damage in the area and it was
63 clearly felt in Northern and Central Italy, up to epicentral distances of ~ 300 km. During the 13 days
64 following the main shock six events with magnitude $M_w > 5$ occurred, peaking on May 29th, with the 5.8
65 M_w events ~ 12 km WSW of the main shock. The seismic sequence of more than 1000 events with a
66 local magnitude $M_l > 3$, lasted for ~ 3 weeks and developed along a south dipping normal fault
67 [Piccinini et al., 2012].

68 Seismic moment for the main shock was 7×10^{24} dyne-cm and relative source time functions
69 calculated for the event show that a great part of the energy was radiated by a source propagating
70 towards WSW, and this would correspond to an oblique, down-dip rupture propagation [Piccinini et al.,
71 2012]. However, the azimuthal distribution of the relative source time functions (RSTF) amplitude

72 suggests a more complex pattern of rupture propagation, which was interpreted in terms of a secondary
73 rupture front, which propagated towards the East, roughly parallel to the fault strike [Piccinini et al.,
74 2012].

75 The observed extensive damage is partly to be explained in terms of seismic site effects in the Po
76 Plain syntectonic alluvial basin. Surrounded by the Alps to the north and by the Appennines mountain
77 ranges to the south, the Po Plain is filled with Plio-Pleistocene sediments, with depths varying from
78 few hundred meters to several kilometers. Amplification of seismic ground-shaking was observed for
79 frequencies between 0.5 and 1.5 Hz, as a consequence of the shallow sediments [Bordoni et al., 2012;
80 Priolo et al., 2012].

81

82

83 **3. Infrasound array observation of the M_w 5.9 earthquake**

84 Infrasound from the main shock was clearly recorded at the CHA infrasound array deployed at a
85 source-to-receiver distance of 294 km from the earthquake epicenter (Figure 1a). The CHA infrasound
86 array is a small aperture (~ 140 m), 4-elements array, deployed at an elevation of ~ 2000 m a.s.l. in
87 Champoluc (AO), in the Northwestern Italian Alps (Figure 1a). The array is equipped with 4
88 OptimicTM 2180 microphones, with a sensitivity of 100 mV/Pa, a low-pass cutoff frequency of 0.5 Hz
89 and instrumental self-noise of -70 dB (relative to 1 Pa²/Hz @ 1 Hz).

90 On May 20th, 2012, around 02:05 UTC, the four microphones of the CHA array detected the
91 seismic shaking of the ground, that was followed, approximately ten minutes later (02:15 UTC), by a
92 long lasting infrasonic signal (Figure 1b). The seismic wave took approximately 40 seconds to
93 propagate 294 km from the epicenter to the array, with a mean propagation velocity of 7.3 km/s
94 consistent with the Moho discontinuity refracted p wave arrival.

95 Infrasound produced by the earthquake is recorded between 02:15 and 02:27 UTC as an emergent
96 spindle-shaped signal of long duration, with a peak amplitude of 0.1 Pa in the 1-3 Hz frequency band
97 (Figure 1b,c). The array analysis indicates a continuous arrival of infrasound detected with a stable
98 apparent velocity of ~ 340 m/s and varying back-azimuth (spanning $\sim 30^\circ$) for the whole emergent
99 long-lasting signal (Figure 1d). The tail of the infrasonic wave-packet is showing an amplitude
100 modulation possibly reflecting multiple sources or arrivals with varying energy from an extended
101 source. This second hypothesis is more consistent with the observed smooth variation of infrasound
102 back-azimuth and stable spectral content.

103 The timing of the infrasound detections (02:15-02:27 UTC) with respect to the earthquake onset
104 time (02:03 UTC) is not consistent with infrasound being radiated only at the epicenter. At a source-to-
105 receiver distance of 296 km in fact, the corresponding celerity would span between 205 m/s for late
106 detections around 02:27 and 410 m/s for early detections around 02:15 UTC (Figure 1b). Here, only
107 infrasound recorded around 02:20 UTC with back-azimuth of $\sim 110^\circ\text{N}$ pointing to the earthquake
108 epicenter appears consistent with a celerity of ~ 300 m/s, thus suggesting stratospheric arrivals of
109 primary infrasound produced at the epicenter. This timing of infrasound detections is rather suggesting
110 the complex generation of infrasound from both primary and secondary sources.

111 Moreover, while propagation velocity is extremely stable at 340 m/s, back-azimuth is actually
112 showing a large variation up to 30° (Figure 1d) from the real back-azimuth to the earthquake epicenter
113 (110°N). Back-azimuth is observed to increase from the initial value of $\sim 90^\circ\text{N}$ (around 02:15 UTC)
114 moving southward up to a maximum value of 110°N (around 02:20 UTC), and to decrease back to
115 $\sim 95^\circ\text{N}$ at the end (around 02:27 UTC) of the emergent phase (Figure 1d). Such a large azimuth
116 variation is the evidence of an extended radiant area for the recorded infrasound.

117

118

119 **4. Modeling the source area by FDTD analysis**

120 In order to evaluate the area of maximum infrasound radiation, we followed the procedure
 121 described by Arrowsmith et al., [2009] and modeled the infrasound source area from the timing and
 122 back-azimuth of infrasound detections at the CHA array (Figure 1c), in terms of ground-to-atmosphere
 123 coupling of seismic waves. Here, seismic waves are assumed to radiate spherically from the earthquake
 124 hypocenter, propagating in the ground at constant velocity and then coupling to the atmosphere to
 125 propagate as infrasound. Hypocentral location ($\lambda_e = 44.896$, $\varphi_e = 11.264$, $h_e = 9.5$ km) and origin time
 126 of the event ($t_e = 02:03:50$ UTC) are given by accurate seismic location by the Italian national seismic
 127 network. The infrasound source area is identified with a grid searching procedure, which minimizes the
 128 difference between real and modeled back-azimuth and arrival time of infrasound detections.

129 The searching grid of 71x165 nodes covers Northern Italy, extending 4 degrees in latitude and 8
 130 degrees in longitude and with a grid spacing of 0.05 degrees. We assume each node (i,j) of the grid as
 131 being a possible source of infrasound due to ground coupling of the seismic wave within the
 132 atmosphere and calculate the expected back-azimuth at the array (az_{ij}) and the seismo-infrasonic travel
 133 time (t_{ij}), with a seismic wave propagating from the hypocenter to the grid node (i,j) at steady velocity
 134 and infrasound wave propagating from the grid node to the array along great-distance circles.

135 The expected back-azimuth of each grid node (i,j) from the array (az_{ij}) is evaluated directly from
 136 the great-circle bearing angle for a spherical earth:

137

138
$$az_{ij} = \tan^{-1} \left[\frac{\sin(\varphi_a - \varphi_{ij}) \cos(\varphi_a)}{\cos(\lambda_{ij}) \sin(\lambda_a) - \sin(\lambda_{ij}) \cos(\lambda_a) \cos(\varphi_a - \varphi_{ij})} \right], \quad (\text{eq.1})$$

139

140 being λ_{ij} and φ_{ij} the latitude and longitude of a given point (i,j) of the searching grid and λ_a and
 141 φ_a the coordinates of the central element of the array. Possible ray deflection due to transverse winds
 142 is neglected here.

143 The travel time from the hypocenter to the array (t_{ij}) is calculated as the sum of the seismic travel
 144 time from the hypocenter to each node of the searching grid (t_{sij}) and the infrasonic travel time from
 145 the node to the array (t_{ij}) .

146

$$147 \quad t_{ij} = t_{sij} + t_{ij}. \quad (\text{eq. 2})$$

148

149 In order to evaluate the seismic travel-time for each node (t_{sij}) we assumed spherical
 150 propagation from a point source located at the earthquake hypocenter $(\lambda_e, \varphi_e, h_e)$ into a homogeneous
 151 half-space with constant velocity of 5.8 km/s. This value is in accordance with first arrivals recorded at
 152 seismic stations of the Italian National Seismic Network up to distances of 150 km from the source and
 153 represents the mean velocity in the crust [Piccinini et al., 2012]. Here, any directivity of the source or
 154 heterogeneity of the medium is neglected. This assumption is however of minor importance, being the
 155 seismic propagation velocity one order of magnitude larger than the sound propagation velocity in the
 156 atmosphere, thus the uncertainty of the velocity structure in the crust has a limited effect on the
 157 modeled timing of the infrasound detection (t_{ij}) .

158 The infrasonic travel-time from the grid to the CHA array (t_{ij}) is obtained with a 2D FTDT
 159 modeling [De-Groot-Hedlin et al., 2011; Lacanna et al., 2014] of the pressure wave propagation in the
 160 atmosphere, in order to account for wind effects and atmospheric profile. In particular, the 2D FTDT
 161 analysis was applied on 36 profiles centered in the CHA array and spaced by 10 degrees along great
 162 circle distances and covering the whole area of the searching grid. Total length of the profiles spans
 163 from a minimum of 84 km for the section with back-azimuth of 270 °N to a maximum of 580 km for

164 section with back-azimuth of 110 °N. Wind, temperature and density for each section from the ground
 165 up to an elevation of 70 km are obtained by interpolating ECMWF High-Resolution atmospheric model
 166 (HRES) analysis at 91 mean pressure levels up to 0.01 hPa (L91) with a spectral resolution of ~12 km.
 167 for the time of occurrence of the event and for the area of analysis.

168 For each section, a Gaussian-shaped pulse with a frequency of 0.2 Hz was used as the source time
 169 function for the 2D FDTD modeling and a lattice grid size of 25 m was applied with a time
 170 discretization of 0.0156 seconds, which satisfies the stability conditions of the FDTD. Here, the
 171 infrasonic travel-time to the array is calculated every 5 km along each section (Figure 2). Results
 172 obtained for all the 36 profiles are then interpolated across the searching grid and the corresponding
 173 infrasonic travel-times (t_{ij}) are evaluated. The seismo-infrasonic travel time (t_{ij}) is eventually
 174 calculated over the whole searching grid (2c) by adding the seismic (t_{sij}) and infrasonic (t_{ij})
 175 counterparts. 2D FDTD modeling predicts direct arrivals for short distances and stratospheric arrivals
 176 for longer sections, with maximum seasonal wind blowing to the west at an altitude of about 50 km
 177 strongly modifying infrasonic travel times from spherical symmetry along east-west profiles (Figure 2,
 178 Figure 3a).

179 For each infrasonic detection at the CHA array, we measured the back-azimuth (az_d) and the
 180 travel time $dt_d = t_d - t_e$, as the difference between the timing of the infrasound detection (t_d) and the
 181 origin time of the earthquake (t_e) as provided by the independent seismic event location.

182 In order to evaluate the most probable position of the source of each infrasound detection (d), the
 183 normalized difference between the observed and theoretical values of back azimuth ($dAZ_d(i,j)$) and
 184 travel time ($dT_d(i,j)$) are evaluated:

185

$$186 \quad \begin{cases} dAZ_d(i,j) = \frac{|az_{ij}-az_d|}{\max(|az_{ij}-az_d|)} \\ dT_d(i,j) = \frac{|t_{ij}-dt_d|}{\max(|t_{ij}-dt_d|)} \end{cases}, \quad (\text{eq. 3})$$

187

188 for each node (i,j) of the grid leading to matrices with values ranging between 0 and 1. When the
189 node (i,j) coincides with the position of the real source the difference between theoretical and measured
190 azimuth $(az_{ij}-az_d)$ and travel time $(t_{ij}-dt_d)$ will be zero. Therefore, the node with the lowest values of
191 dAZ_d and dT_d will most probably represent the position of the infrasonic source of a given detection (d).

192 In order to account for both back-azimuth and travel time in the searching procedure, the two
193 matrices are eventually multiplied ($M_d(i,j) = dAZ_d(i,j) \times dT_d(i,j)$) leading to a matrix with values
194 ranging between 0 and 1, and the possible source position of secondary infrasound is identified in the
195 node of the grid (i_{do}, j_{do}) where the matrix $M_d(i,j)$ is minimum (Figure 3b).

196 All the minima evaluated for all the infrasound detections are then combined in a single map, that
197 represents the whole infrasound radiation area (Figure 3b) induced by seismic wave coupling to the
198 atmosphere. The result highlights an extended area of infrasound radiation, that from the epicenter
199 develops for ~100 km to the east along the Po river up to the Po delta, while develops ~100/150 km
200 toward the north-west up to the Garda Lake and the Alpine mountain range (Figure 3b).

201

202

203 **5. Modeling the source area by back-projection of infrasound back-azimuth**

204 In addition to the procedure presented above, a location of infrasound detections was performed,
205 considering stratospheric arrivals and transverse wind effects on the propagation path. Detections after
206 02:25 UT were not considered. Assuming these detections produced from seismic waves originated
207 from the epicenter (not from a spatially extended source), the corresponding locations are found over
208 sea unless considering unrealistic celerity values (<0.2 km/s).

209 Ray-tracing simulations using the WASP-3D ray theory-based method which account for the the
210 spatiotemporal variations of the horizontal wind terms along the ray paths [Virieux et al., 2004] and the

211 ECMWF analyses, were performed assuming a source altitude of 1 km, slowness values ranging
212 between 2.6 and 3 s/km. 200 rays were launched with incidence angle equally spaced. Simulations
213 predict a dominant stratospheric waveguide with a refracting height up to 44-54 km altitude, being
214 characterized by a celerity of 0.295 and 0.305 km/s and azimuthal deviation ranging from -4° to 3°
215 depending on the ray trajectory.

216 The location of the infrasound sources are calculated using an inverse location procedure which
217 combines the seismic source information (epicenter coordinates and origin time), celerity models both
218 infrasound and seismic waves, and the arrival times and wind-corrected azimuth of infrasound waves
219 [e.g. Le Pichon et al., 2002]. The location of each detected infrasonic signal is then back-projected on
220 its back-azimuth with a distance constrained by seismic propagation time from the hypocenter to any
221 source point and travel time through the atmosphere from the source point to CHA. Taking into account
222 the propagation variability due to atmospheric uncertainties and errors in the wave front measurements
223 taking into account the station geometry, a maximum location error of $\sim \pm 25$ km is estimated
224 [Szuberla and Olson, 2004; Le Pichon et al., 2015].

225 Using these simulation results, assuming stratospheric arrivals, a density map of infrasound
226 detections is obtained (Figure 3c). This results into a good agreement with the map obtained with
227 FDTD analysis and identify an extended area of infrasound radiation, which from the earthquake
228 epicenter extends to the east up to the delta of PO river and to the north-west up to the Garda lake and
229 the southern margin of the Alpin chain.

230

231

232 **6. Discussion and conclusions**

233 The analysis of infrasound detections at the CHA array, combined with the seismological
234 information available on the location and origin time of the May, 20th, 2012 Ferrara earthquake,

235 allowed to identify a 200 km extended source area of infrasound, spanning from the southern flank of
236 Alpine chain to the north-east ($\lambda=46^\circ$, $\varphi=10^\circ$), to the delta of Po river ($\lambda=45^\circ$, $\varphi=12.5^\circ$) to the east
237 (Figure 3) and showing a preferential distribution in the East-West direction from the epicenter to the
238 coastline. Results obtained from FDTD analysis of pressure wave propagation in the atmosphere
239 (Figure 3b) and back-projection of wind-corrected azimuth of infrasound waves (Figure 3c) are highly
240 consistent with each other. Such an extended radiant area is in agreement with the long lasting
241 infrasonic signal and the observed variations of back-azimuth (Figure 1b, d) and might also explain the
242 observed amplitude modulation of the infrasonic wave-packet. Infrasound produced at the epicenter is
243 recorded with a back-azimuth of 110°N around 02:20 UTC, consistent with a celerity of 300 m/s for
244 the epicentral distance of ~ 300 km. Infrasound radiated from the most western portion ($\sim 90^\circ\text{N}$) of the
245 area is recorded few minutes before the epicentral infrasound (around 02:15 UTC), as a consequence of
246 the shortest distance (~ 200 km) to the array. In the same way, infrasound radiated east of the epicenter,
247 is recorded with a back-azimuth of $\sim 95^\circ\text{N}$ few minutes after the epicentral infrasound (around 02:27
248 UTC), as a consequence of the longer distance (~ 400 km) traveled by the infrasonic wave. The
249 radiation area is clearly limited to the coastline to the east, being ground-to-atmosphere coupling of
250 seismic waves unlikely in the sea, and reported up-to-now only for major earthquake [Evers et al.,
251 2014]. This result is a good validation of the proposed modeling.

252 It is worth noting that the area of maximum infrasound radiation modeled from our infrasound
253 observation is actually confined within the Po plan, with no significant infrasound radiated by the
254 Alpine and/or Appenines mountain ranges that are actually boarding the Po plain to the north and to the
255 south. We can consider the whole Po plan as almost immediately shacking for the earthquakes, with
256 seismic waves inducing infrasound in the atmosphere. We suggest therefore that the ground shaking of
257 the Po plan is the most likely source mechanism of the secondary infrasound. This hypothesis is
258 corroborated by the spectral content of recorded infrasound (1-2 Hz) peak frequency, that is consistent

259 with the (0.5-1.5 Hz) peak frequency of the ground-shaking in the PO plan as the effect of the
260 amplification effects due to the soft sediments of the PO valley [Priolo et al., 2012; Bordoni et al.,
261 2012].

262 This conclusion differs significantly from previous studies [Le Pichon et al., 2003; Arrowsmith et
263 al., 2009; Green et al., 2009], where secondary infrasound was strongly related to topographic relief,
264 while it appears consistent with the work of Walker et al., [2013], where both enhanced topography and
265 flat areas were identified from infrasound observations from the Tohoku earthquake. Anyway, based
266 on our observations we can conclude that the Po plain shaking was definitely the most energetic source
267 of the infrasonic observed detections.

268 Infrasound detections of the main shock are compared with infrasound detection for the most
269 energetic aftershock (2012/05/29, $M_l=5.8$) recorded during the 2012 seismic sequence (Figure 4). In
270 both cases infrasound detections show the same pattern of back-azimuth variation with time and delay
271 from the earthquake onsets, confirming the modeled extended source mechanism. Figure 4 suggests
272 also how infrasound detections from source areas far from the earthquake epicenter (i.e. recorded
273 before minute 10 or after min 20 from the earthquake epicenter) might depend on the magnitude and
274 depth of the event.

275 In order to analyze the mechanism of secondary infrasound radiation by the earthquake, we
276 compared the modeled radiant area, obtained both from FDTD analysis (Figure 3b) and back-projection
277 of wind-corrected azimuth of infrasonic waves (Figure 3 c), with shake map and the acoustic effect of
278 the event (Figure 3d). Earthquake booms have been reported for a long time [Michael, 2011 for a
279 review] and are commonly explained as being produced by the refraction of the “p” wave into the
280 atmosphere very close to the listener. The map is obtained interpolating 8766 reports distributed over
281 1645 municipalities and shows the percentage of earthquake booms felt in a given municipality with
282 respect of the number of reports. The map of earthquake boom shows how the earthquake boom was

283 clearly felt in a wide area extending from the shoreline to the west, where ~70% of the people reporting
284 the event felt a clear earthquake boom, towards the Alpine mountain chain to the north-east, where
285 ~45% of the people reported the earthquake boom at distances of ~ 200 km from the epicenter. For
286 epicentral distances exceeding 250-300 km this effect is minimal in all directions. Similarly, the shake
287 map of the event, derived from ~ 120 accelerometer record of the Italian National Network (RAN),
288 confirms maximum peak ground acceleration in the epicentral area as well as enhanced ground
289 acceleration North/West and East of the epicenter, in good agreement with the earthquake boom.

290 We suggest that the good match observed between seismic observation of the event (seismic
291 shake map and map of felt earthquake boom) and the modeled area of maximum infrasound radiation
292 (Figure 3d) is confirming our finding of infrasound being mostly radiated in the alluvial plan. In this
293 context infrasound radiation appears to be controlled by the local shallow geology, with the east-west
294 extension of the infrasonic source area from the epicenter (Figure 3b,c) to the coastline matching the
295 position of the Po and Adige rivers in the alluvial plan, whose recent deposits are sites of maximum
296 seismic amplifications and are characterized by enhanced peak ground acceleration and acoustic effect
297 of the earthquake (Figure 3d). At the same time however, this preferential trend is in agreement with
298 the geometry of the fault plane, thus possibly suggesting a source effect of the geometry and extend of
299 the infrasound radiant area.

300

301 **7. Data and Resources**

302 Infrasound data of the May, 20th, 2012 Ferrara earthquake have been recorded a permanent
303 infrasound array operated in Champoluc (AO, Italy) by the Department of Earth Sciences of the
304 University of Firenze. Raw infrasound data are freely available upon request to the corresponding
305 author. Location and occurrence time of the earthquake is obtained from the Italian seismological
306 instrumental and parametric data-base (ISIDE, <http://iside.rm.ingv.it/iside/standard/index.jsp>). Data of

307 earthquake boom are obtained from the database of the Istituto Nazionale di Geofisica e Vulcanologia
308 (<http://www.haisentitoilterremoto.it/>). Accelerometer data of the event, used for the shake map, are
309 obtained from the database of the National Accelerometer Network
310 (<http://www.protezionecivile.gov.it/jcms/it/ran.wp>).

311

312 **8. Acknowledgements**

313 This work was supported by the European Union ARISE FP7 project (GA 284387). We
314 acknowledge the editor and two anonymous reviewers for their comments.

315

316

317 **9. References**

318 Arrowsmith, S. J., R. Burlacu, R. Whitaker, and G. Randall (2009). A repeating secondary
319 source of infrasound from the Wells, Nevada, earthquake sequence. *Geophys. Res. Lett.*, 36,
320 L11817. doi:10.1029/2009GL038363.

321 Bordoni, P., R. M. Azzara, F. Cara, R. Cogliano, G. Cultrera, G. Di Giulio, A. Fodarella,
322 G. Milana, S. Pucillo, G. Riccio, A. Rovelli, P. Augliera, L. Luzi, S. Lovati, M. Massa, F.
323 Facor, R. Puglia, G. Ameri (2012), Preliminary results from EMERISTO, a rapid response
324 network for site-effect studies. *Annals of Geophysics*, 55(4), 599-607, doi:10.4401/ag-6153.

325 de Groot-Hedlin, C., M. A. H. Hedlin, and K. Walker (2011), Finite difference of
326 infrasound propagation through a windy, viscous atmosphere: Application to a bolide explosion
327 detected by seismic networks, *Geophys. J. Int.*, 185, 305–320, doi:10.1111/j.1365-
328 246X.2010.04925.x.

- 329 Evers, L. G., D. Brown, K. D. Heaney, J. D. Assink, P. S. M. Smets, and M. Snellen
330 (2014), Evanescent wave coupling in a geophysical system: Airborne acoustic signals from the
331 Mw 8.1 Macquarie Ridge earthquake, *Geophys. Res. Lett.*, 41, 1644–1650,
332 doi:10.1002/2013GL058801
- 333 Green, D., J. Guilbert, A. Le Pichon, O. Sebe, and D. Bower (2009), Modelling Ground-
334 to-Air Coupling for the Shallow ML4.2 Folkestone, UK, Earthquake of 2007 April 28. *Bull.*
335 *Seism. Soc. Am.*
- 336 Lacanna, G., M. Ichihara, M. Iwakuni, M. Takeo, M. Iguchi, and M. Ripepe (2014),
337 Influence of atmospheric structure and topography on infrasonic wave propagation, *J. Geophys.*
338 *Res. Solid Earth*, 119, 2988–3005, doi:10.1002/2013JB010827.
- 339 Le Pichon, A., J. Guilbert, M. Vallée, J.X. Dessa, and M. Ulziibat (2003), Infrasonic
340 imaging of the Kunlun Mountains during the great 2001 China earthquake. *Geophys. Res. Lett.*,
341 DOI:10.1029/2003GL017581.
- 342 Le Pichon, A., J. Guilbert, A. Vega, M. Garcés, and N. Brachet (2002), Ground-coupled
343 air waves and diffracted infrasounds from the Arequipa earthquake of June 23, 2001, *Geophys.*
344 *Res. Lett.*, 1029/2002GL015052.
- 345 Le Pichon, A., P. Herry, P. Mialle, J. Vergoz, N. Brachet, and M. Garcés (2005),
346 Infrasound associated with 2004-2005 large Sumatra earthquakes and tsunami. *Geophys. Res.*
347 *Lett.*, 32, L19802, doi:10.1029/2005GL023893.
- 348 Le Pichon, A., J. D. Assink, P. Heinrich, E. Blanc, A. Charlton-Perez, C. F. Lee, P. Keckhut, A.
349 Hauchecorne, R. Rüfenacht, N. Kämpfer, et al. (2015), Comparison of co-located independent ground-

350 *based middle atmospheric wind and temperature measurements with numerical weather prediction*
351 *models, J. Geophys. Res. Atmos., 120, 8318–8331, doi:[10.1002/2015JD023273](https://doi.org/10.1002/2015JD023273).*

352 Michael, A. J. (2011), Earthquake sounds: In Encyclopedia of solid earth geophysics,
353 Springer, pp. 188-192, doi:10.1007/978-90-481-8702-7_201, Dordrecht, The Netherlands.

354 Mutschlecner, J. P., and R. W. Whitaker (2005), Infrasound from earthquakes. *J.*
355 *Geophys. Res.*, 110, D01108, doi:10.1029/2004JD005067.

356 Olson, J. V., C. R. Wilson, and R. A. Hansen (2003), Infrasound associated with the 2002
357 Denali fault earthquake, Alaska. *Geophys. Res. Lett.*, 30(23) 2195, 1-4,
358 doi:10.1029/2003GL018568.

359 Piccinini, D., N. A. Pino, and G. Saccorotti (2012), Source complexity of the May 20,
360 2012, MW 5.9, Ferrara (Italy) event. *Annals of Geophysics*, 55(4), doi:10.4401/ag-6111.

361 Priolo, E., M. Romanelli, C. Barnaba, M. Mucciarelli, G. Laurenzano, L. Dall'Olio, N.
362 Abu Zeid, R. Caputo, G. Santarato, L. Vignola, C. Lizza, P. Di Bartolomeo (2012), The Ferrara
363 thrust earthquakes of May-June 2012: preliminary site response analysis at the sites of the OGS
364 temporary network. *Annals of Geophysics*, 55(4), doi:10.4401/ag-6172.

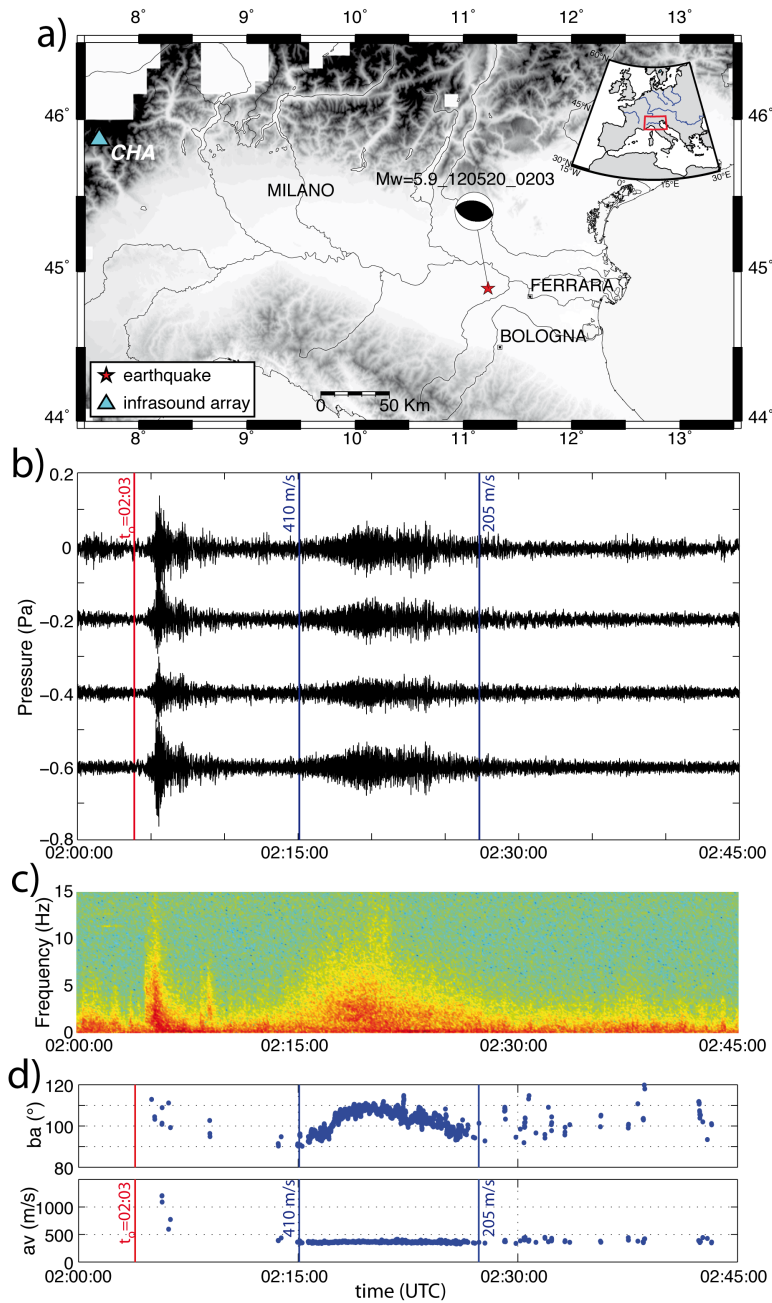
365 Szuberla, C. A. L., and J. V. Olson, 2004, Uncertainties associated with parameter
366 estimation in atmospheric infrasound arrays, *J. Acoust. Soc. Am.* 115, 253–258,
367 <http://dx.doi.org/10.1121/1.1635407>

368 Virieux, J., Garnier, N., Blanc, E. & Dessa, J.X., 2004. Paraxial raytracing for
369 atmospheric wave propagation, *Geophys. Res. Lett.*, 31, doi:10.1029/2004GL020514

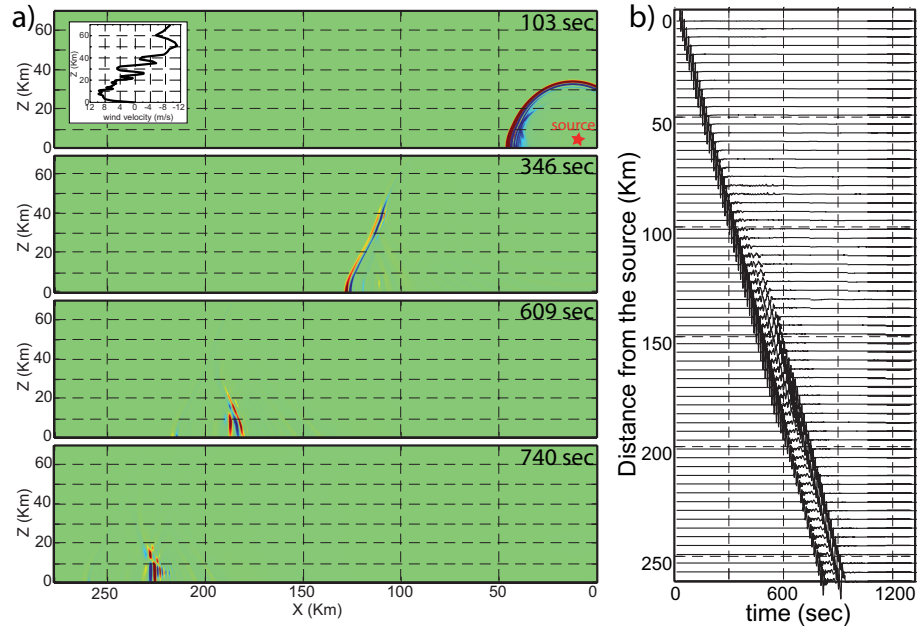
370 Walker, K. T., A. Le Pichon, T. S. Kim, C. de Groot-Hedlin, I.-Y. Che and M. Garcés
371 (2013), An analysis of ground shaking and transmission loss from infrasound generated by the
372 2011 Tohoku earthquake, *J. Geophys. Res. Atmos.*, *118*, 12,831-12,851,
373 doi:10.1002/2013JD020187.

374

Figure Captions



377 Figure 1: (a) Epicenter of the May, 20th, 2012 Ferrara earthquake (red star) and position of the CHA
 378 infrasound array (blue triangle) at a distance of ~300 km from the earthquake epicenter. Raw infrasound data (b)
 379 and spectrogram (c) recorded at the CHA array. (d) back-azimuth (ba) and apparent velocity (av) of infrasound
 380 detections obtained for the infrasonic signal at the CHA array. Earthquake origin time (red line) and celerity
 381 values that would correspond to early and late arrivals (410 and 205 m/s, blue lines) are shown for reference.



382

383

Figure 2: FDTD analysis of infrasound propagation along the 180° N atmospheric profile to the array.

384

Snapshots of the infrasound propagation at 103, 346, 609 and 740 seconds respectively (a). Synthetic

385

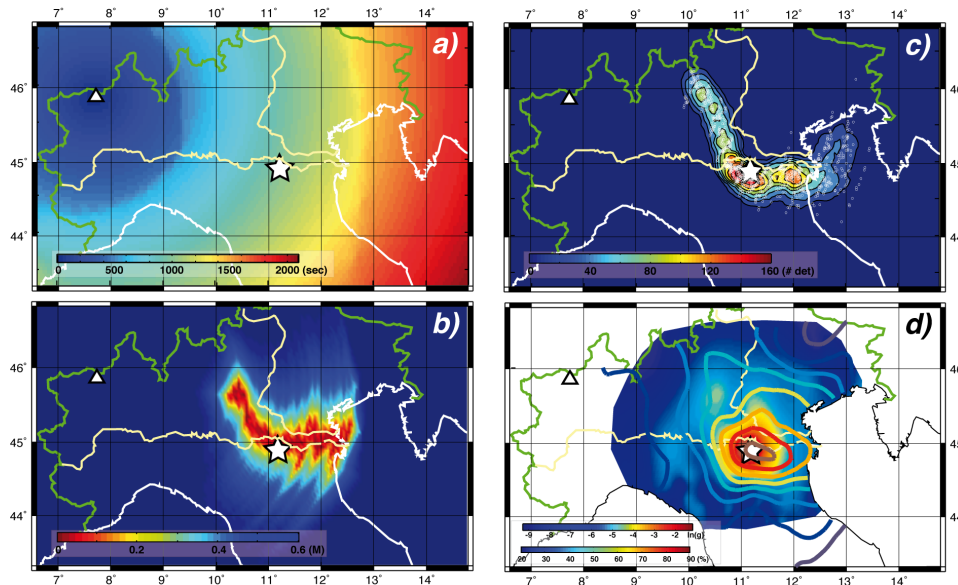
waveforms evaluated at ground level every 5 km along the profile (b). Waveforms are amplitude normalized in

386

order to enhance the arrival time and show stratospheric arrivals at distances exceeding 130-150 km from the

387

source.



388

389

Figure 3: Theoretical seismo-acoustic travel-time (a) of infrasound radiated by secondary sources

390

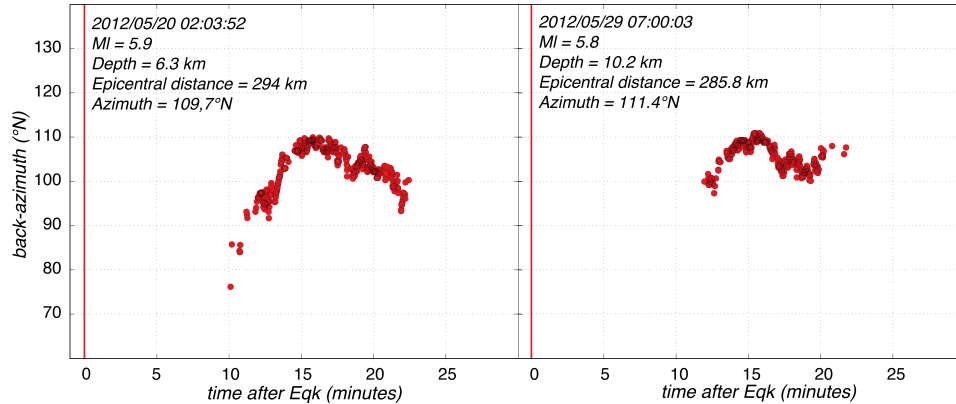
positioned in the different nodes of the searching grid as it would be recorded by the CHA array. Modeled

391

infrasound radiation area (b) for the main May, 20, 2012, event obtained by combining differences in expected

Infrasound by earthquake interaction with alluvial sediment

392 and observed back-azimuth and travel times (a) for all the infrasound detections of the earthquake. (c) Location
393 (white circles) and density map of infrasonic sources based on ray-tracing. (d) Distribution of earthquake booms
394 felt in northern Italy (contour-lines) and shake map (colored map) for the 2012, May 20th event.. Contour-lines
395 represent the percentage of felt boom within the total number of reports. In all subplots position of the
396 earthquake epicenter (white star) and of the CHA array (white triangles) is shown as well as national border
397 (green line) coastline (white line) and the main rivers (yellow lines).



398

399 Figure 4: Infrasound detections of the infrasound produced by the May 20th, 2012 main shock (MI 5.9) and
400 by the May, 29th, 2012 aftershock (MI 5.8). The time of the infrasound detections is expressed in terms of
401 minutes after the earthquake occurrence time.